Annals of Biomedical Engineering, Vol. 39, No. 4, April 2011 (© 2011) pp. 1349–1357
DOI: 10.1007/s10439-011-0269-6

Spatial Frequency Domain Imaging of Intrinsic Optical Property Contrast in a Mouse Model of Alzheimer's Disease

Alexander J. Lin,[1,2] Maya A. Koike,[2] Kim N. Green,[2] Jae G. Kim,[1] Amaan Mazhar,[1] Tyler B. Rice,[1] Frank M. LaFerla,[2] and Bruce J. Tromberg[1]

[1]Laser Microbeam and Medical Program (LAMMP), Beckman Laser Institute and Medical Clinic, 1002 Health Sciences Road, Irvine, CA 92612, USA; and [2]UC Irvine Institute for Memory Impairments and Neurological Disorders (UCI MIND), 2642 Biological Sciences III, Irvine, CA 92697-4545, USA

(*Received 13 September 2010; accepted 3 February 2011; published online 19 February 2011*)

Associate Editor Angelique Louie oversaw the review of this article.

Abstract—Extensive changes in neural tissue structure and function accompanying Alzheimer's disease (AD) suggest that intrinsic signal optical imaging can provide new contrast mechanisms and insight for assessing AD appearance and progression. In this work, we report the development of a wide-field spatial frequency domain imaging (SFDI) method for non-contact, quantitative *in vivo* optical imaging of brain tissue composition and function in a triple transgenic mouse AD model (3xTg). SFDI was used to generate optical absorption and scattering maps at up to 17 wavelengths from 650 to 970 nm in 20-month-old 3xTg mice ($n = 4$) and age-matched controls ($n = 6$). Wavelength-dependent optical properties were used to form images of tissue hemoglobin (oxy-, deoxy-, and total), oxygen saturation, and water. Significant baseline contrast was observed with 13–26% higher average scattering values and elevated water content ($52 \pm 2\%$ vs. $31 \pm 1\%$); reduced total tissue hemoglobin content (127 ± 9 μM vs. 174 ± 6 μM); and lower tissue oxygen saturation ($57 \pm 2\%$ vs. $69 \pm 3\%$) in AD vs. control mice. Oxygen inhalation challenges (100% oxygen) resulted in increased levels of tissue oxy-hemoglobin (ctO_2Hb) and commensurate reductions in deoxy-hemoglobin (ctHHb), with ~60–70% slower response times and ~7 μM vs. ~14 μM overall changes for 3xTg vs. controls, respectively. Our results show that SFDI is capable of revealing quantitative functional contrast in an AD model and may be a useful method for studying dynamic alterations in AD neural tissue composition and physiology.

Keywords—Structured light, Vascular reactivity, Hyperoxia, *In vivo* spectroscopy, Microvascular perfusion, Diffuse optical imaging, Scattering, Absorption, Tissue optical properties.

Address correspondence to Bruce J. Tromberg, Laser Microbeam and Medical Program (LAMMP), Beckman Laser Institute and Medical Clinic, 1002 Health Sciences Road, Irvine, CA 92612, USA. Electronic mail: bjtrombe@uci.edu

INTRODUCTION

More than 35 million people world-wide have Alzheimer's disease (AD), a neurodegenerative disease characterized by amyloid-beta (Aβ) plaque and neurofibrillary tau tangle accumulation accompanying neuron death.[31] The cause of sporadic AD, accounting for 85% of cases, is unknown, but increasing evidence is revealing diverse co-factors may all lead to the pathological neurodegeneration seen in AD.[26] Vascular diseases such as atherosclerosis, diabetes mellitus, and stroke are major risk factors. Cerebral stroke alone increases AD prevalence in elderly patients twofold. Hypoxia, which can be caused by hypoperfusion from atherosclerosis or sleep apnea, is shown *in vitro*, in *ex vivo* human brain and *in vivo* animal models to increase Aβ production and inhibit degradation and clearance.[44] These studies give evidence that vascular dysfunction and Aβ pathology are closely intertwined.

In the last 10 years, imaging research using laser speckle,[33] transcranial doppler,[34,36,40] fMRI,[18,43] PET,[37] and SPECT[30] techniques have all described impaired vascular reactivity in AD in response to vasodilation challenges. The implication is that AD patients have a diminished ability to vasodilate in response to hypoxia, leading to hypoxic stress in neurons and subsequent Aβ production. Since there is evidence that Aβ oligomers are the damaging species to vascular function,[11,16,27] and it is hypothesized that decreased vascular reactivity induces further amyloid pathology, a vicious cycle might ensue.

Brain imaging offers a unique approach to studying and managing AD without invasive biopsies. However, imaging with resource-limited fMRI, PET, and SPECT for resolving regions of relatively impaired brain metabolism and radiolabeling AD pathology with

expensive dyes (e.g., Pittsburgh compound B) is not feasible for most animal researchers or human patients. Because all patients have unique, dynamic responses, the ideal imaging device would allow frequent, low cost, rapid measurements of brain function without risk.

Tissue optical spectroscopy can provide those features. Non-ionizing radiation is used to measure physiologic function, such as the concentration of oxy- and deoxy-hemoglobin (ctO_2Hb and ctHHb) (indicators of perfusion and metabolism), tissue oxygen saturation, and lipid and water content at an arbitrary number of time points.[6,39] In research, intrinsic signal optical imaging, which focuses on hemoglobin oxygenation signals, has been widely used to study hemodynamics in the brain during stroke and seizures.[7,13,22] Other tools including laser speckle[4] and transcranial doppler[23] imaging are used in research and the clinic to measure changes in blood flow.

Spatial frequency domain imaging (SFDI) supplements the imaging repertoire as a wide field, non-contact, intrinsic signal technique capable of measuring tissue absorption and scattering properties on a pixel-by-pixel basis. This is done by imaging the frequency-dependent reflectance of a spatially modulated light source projected onto tissue. Tissue optical properties (i.e., absorption, μ_a, and reduced scattering, μ_s', parameters) are calculated for each source wavelength by fitting the demodulated SFDI signals to a light transport model.[9] Images of intrinsic chromophore concentration including ctO_2Hb, ctHHb, water, and lipid are obtained by analyzing the wavelength dependence of light absorption.

SFDI maps of tissue scattering parameters provide unique structural contrast that complements functional information derived from light absorption. Factors in brain tissue scattering such as cell or organelle swelling from edema[15] and vasodilation from cortical activation[38] have been elucidated *in vivo*. In addition, tissue scattering coefficients have been shown to be elevated in *ex vivo* human AD brain tissue[17] and are highly sensitive to cell death *in vitro*[28] and *ex vivo*.[14] SFDI has been well-characterized for tissue spectroscopy[1,3,8] and it has tomography, depth-sectioning, and fluorescence measurement capabilities.[20,25,42] In this work, we demonstrate that SFDI measurements of absorption and scattering signatures in a transgenic mouse model can be used to differentiate AD pathology from normal aging.

MATERIALS AND METHODS

Animal Model

Alzheimer's triple transgenic (3xTg) mice expressing human APP/PS1/tau genes on a C57/BL6-129svj background express both hallmark lesions of AD, Aβ plaques, and tau tangles. Both protein aggregates are toxic to neurons and microvasculature, making the 3xTg mouse an ideal model for studying neurovascular disease. 3xTg male mice were studied at 20 months of age ($n = 4$) to coincide with the appearance of advanced plaque and tangle pathology. Age-matched C57/BL6-129svj mice ($n = 6$) were used to control for changes due to normal aging. All procedures were performed in accordance with the regulations of the Institutional Animal Care and Use Committee (IACUC) of the University of California, Irvine (protocol no. 2010-2934).

Imaging windows were created under gas mask isoflurane anesthesia (2% maintenance in 21% oxygen balanced by nitrogen) by removing the skin from bregma anteriorly to lambda posteriorly and bilaterally to the temporalis muscle attachments. The mouse skull, 200–700 μm thick, was left intact to reduce trauma artifact from removing or thinning it. This approach has been used widely in intrinsic signal imaging of mouse brain.[13] During the initial surgery and for the imaging session, the mouse was heated by a thermostatically controlled heating pad (*Gaymar*). Immediately after surgery, the mouse's head was secured by adjustable machined ear bars to prevent motion and a thin layer of heavy mineral oil was applied onto the cranium to reduce skull drying.[2,21] Excess gases were scavenged via a *Bickford* adsorber unit and gas flow was maintained at 2.4 L/min.

Steady-State Measurement and Hyperoxia Challenge

An initial 17-wavelength (650–970 nm, every 20 nm) baseline measurement was acquired continuously for 2 min with the mouse breathing 21% O_2 (normoxia). Immediately following the 17-wavelength scan, baseline and dynamic measurements were recorded during an 8 min, 100% oxygen inhalation challenge using only 670 and 850 nm light to achieve a time resolution of about 15 s/measurement while still containing hemoglobin chromophore information. Normoxia was used to measure the baseline optical properties again for 3 min followed by 100% O_2 (hyperoxia) as an experimental perturbation for 5 min. Doing a challenge allowed us to test the brain's reactivity relative to each mouse's baseline values, which reduced the effects of variation in a population of mice. In addition to baseline measurements, it could potentially increase sensitivity to neurovascular defects found in AD mice.

SFDI Instrument and Analysis

A schematic of the experimental arrangement is illustrated in Fig. 1. A complete description of SFDI

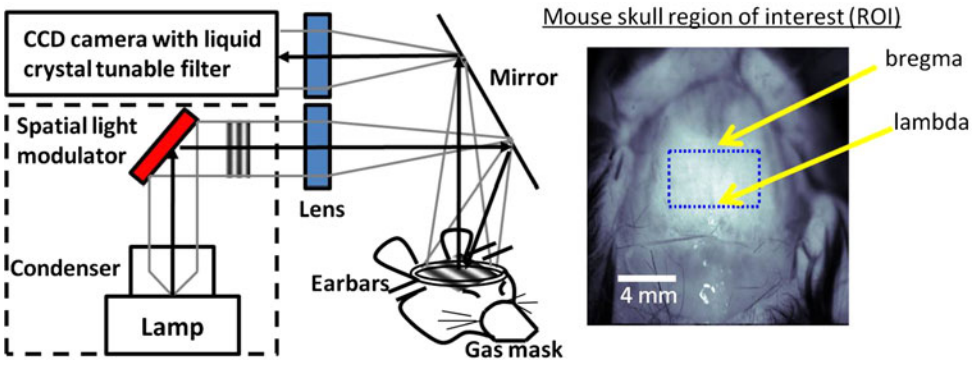

FIGURE 1. (Left) Schematic of SFDI imaging of mouse brain through the intact skull. Non-ionizing broadband light is projected onto a spatial light modulator and light intensity patterns of different spatial frequencies are focused onto the mouse's cranium. The reflectance is captured by a CCD camera with a tunable liquid crystal filter to select for specific wavelengths of light. (Right) Pixels in the region of interest (bregma to lambda and bilaterally to temporalis muscle attachments) are averaged for analyses.

instrumentation and data analysis has been previously presented.[8,9] Briefly, broadband near-infrared (NIR) light from a 250 W quartz-tungsten halogen light source (Newport Corporation, Irvine, CA) was shaped into sinusoidal projection patterns by a computer-controlled DLP Developer's Kit (Texas Instruments, Dallas, TX), consisting of a 1024 × 768 pixel digital micromirror device, and focused by a set of lenses onto the mouse's cranium at a working distance of 750 mm. For both the low AC frequency ($f = 0$ mm^{-1}) and high AC frequency ($f = 0.125$ mm^{-1}), three adjacent light intensity patterns phase-shifted 120° were projected and images were captured across a specified range of wavelengths by a Nuance Multispectral Imaging System (CRI, Inc., Woburn, MA) with a liquid–crystal tunable filter.

The tissue-modulated reflected images at each phase (i.e., I_1, I_2, I_3), consisting of both an AC and DC (Eq. 1) component, were then demodulated to create a composite reflected image for each AC frequency (M_{AC}) with the DC component subtracted out (Eq. 2).

$$I_n = I_n DC + I_n AC \quad (1)$$

$$M_{AC} = \frac{\sqrt{2}}{3}\sqrt{\left((I_1 - I_2)^2 + (I_2 - I_3)^2 + (I_3 - I_1)^2\right)} \quad (2)$$

The final diffuse reflectance image for each frequency was calculated by calibrating to a silicone phantom of known optical properties, which corrects for any system response due to spatial variation of the illumination light and lens aberrations. The mean photon path length in tissue depends on the projected spatial frequency and, hence, recorded light becomes a nonlinear function of this parameter, absorption (μ_a), and reduced scattering (μ_s') coefficients. A known Monte Carlo forward model[8] was then used to create a look-up table for fitting these optical properties on a pixel-by-pixel basis.

Quantitative concentration values of ctO_2Hb, ctHHb, total Hb (ctO_2Hb + ctHHb), tissue oxygen saturation (100 * ctO_2Hb/Total Hb), and percent water were calculated from the absorption spectrum according to the Beer–Lambert law ($\mu_a = 2.3\varepsilon C$, where ε is the known molar extinction coefficient for each chromophore and C is the molar concentration). In addition, the wavelength-dependent scattering was fit to a model based on the Mie theory approximation, $\mu_s' = A\lambda^{-b}$, commonly used in tissue optics, where λ is the optical wavelength and "A" and "b" are free variables determined by a least squares fit.[41]

For each image, the region of interest (ROI) was anatomically standardized between the suture junctions bregma and lambda and bilaterally to the temporalis muscle attachments (Fig. 1). The average and standard deviation (SD) of pixel intensities in the ROI (~5000 pixels) for each mouse were calculated. The within group SD (i.e., 3xTg vs. control) was calculated using the average ROI pixel values for each mouse in the group. All averages, standard error bars, and p values shown were calculated from mean ROI and SD values between animals in each group. A two-tailed student's t test analysis was used to determine significance between Alzheimer's and control mice. All image processing and analyses were done with MATLAB software (Mathworks, Natick, MA).

RESULTS

Baseline Brain Optical Properties

Reduced scattering (μ_s') and absorption (μ_a) images of the brain were determined at 21% O_2 from 650 to 970 nm at 17 wavelengths spaced every 20 nm. Scattering contrast revealed regional differences and was higher in the ROI (red dotted box) in Alzheimer's mice (Fig. 2), while absorption showed a more

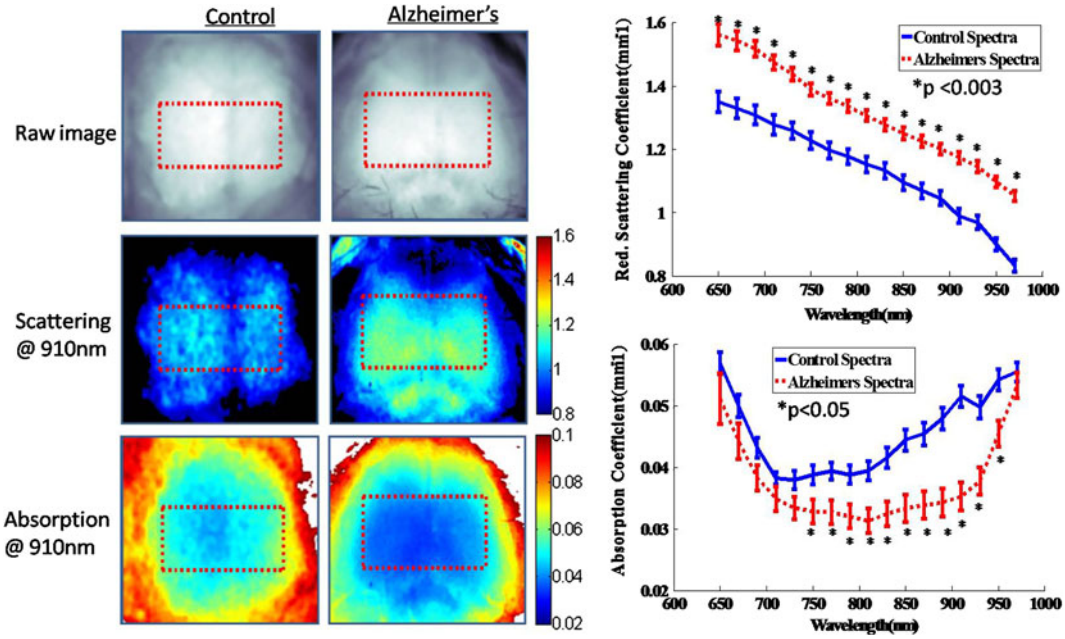

FIGURE 2. Representative optical property maps of control and Alzheimer's brains taken with SFDI *in vivo* at normal air (21% O_2). Pixel values in the ROI were averaged for each mouse and wavelength-dependent reduced scattering and absorption coefficient spectra were plotted for control and 3xTg mice (group average ± group SE).

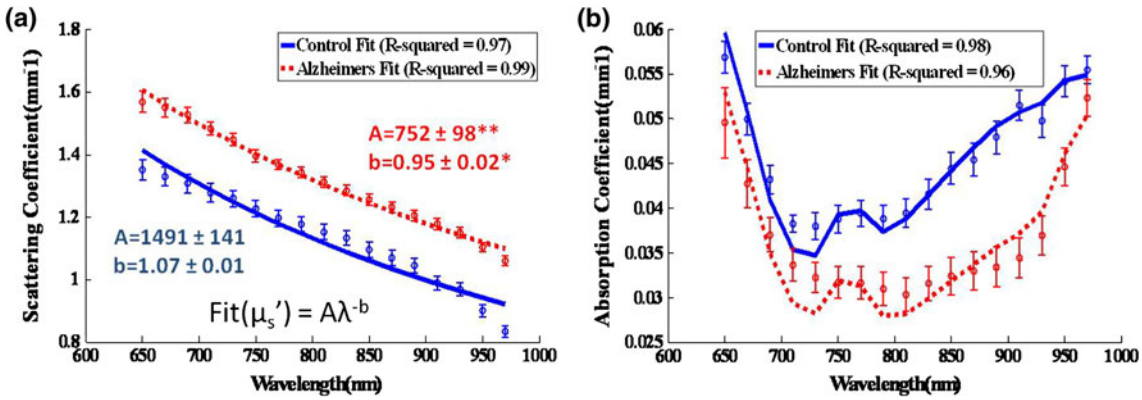

FIGURE 3. (a) Reduced scattering and (b) absorption spectra (group average ± group SE shown) were fit to the Mie scattering power law ($\mu_s' = A\lambda^{-b}$) and for hemoglobin and water chromophores, respectively, with a least squares linear fit and R^2 values were found. *$p < 0.005$, **$p < 0.001$.

homogeneous distribution and was generally lower in Alzheimer's brains. After averaging absorption values in the ROI, the absorption spectrum was noticeably lower in 3xTg mice, especially in the 750–950 nm range ($p < 0.05$). The spectra were fit for hemoglobin and water (Fig. 3) with R^2 values of 0.98 and 0.95 for control and 3xTg mice, respectively. Concentrations of baseline chromophores are summarized in Table 1. AD mice displayed elevated water content (52 ± 2% vs. 31 ± 1%); reduced total tissue hemoglobin content (127 ± 9 μM vs. 174 ± 6 μM); and lower tissue oxygen saturation vs. control mice (57 ± 2% vs.

TABLE 1. Baseline normoxia values of chromophores expressed as (mean ± SE) in control (n = 6) and 3xTg (n = 4) mouse groups.

Subject	ctO_2Hb (μM)	ctHHb (μM)	Total Hb (μM)	O_2 sat (%)	Water (%)
Control 17wv	119 ± 6	55 ± 2	174 ± 6	69 ± 2	31 ± 2
3xTg 17wv	73 ± 6**	54 ± 4	127 ± 9**	57 ± 2**	52 ± 1**

Values determined from fits to 17 wavelength SFDI absorption spectra (650–970 nm).
**$p < 0.003$.

69 ± 2%). Scattering was also significantly higher (13–26%) in 3xTg mice for all 17 wavelengths ($p < 0.003$), confirming a previous *ex vivo* human study of AD brain tissue.[17] The wavelength-dependent scattering was fit to the Mie theory approximation with R^2 values of 0.97 and 0.99 for control and 3xTg mice, respectively. Scattering pre-factor (A) and power (b) values from the fits showed significant contrast at baseline (Fig 3a).

With 670 and 850 nm acquisition data, chromophore and scattering levels were determined by 3 min baseline average values when the mice were breathing 21% O_2 and after a new steady state was established with 100% O_2 gas mixtures. At normoxia (21% O_2), the baseline chromophore concentrations calculated from the 670/850 nm data were close to the 17-wavelength spectral fits, differing an average of 5% in chromophore values for controls. Notably, and just in 3xTg mice, average ctO_2Hb level was much higher than in the 17-wavelength fits (100 μM vs. 73 μM), which affected the Total Hb and O_2 saturation calculations. Water was not fit for because 670 and 850 nm absorption mainly has contributions from ctHHb and ctO_2Hb, respectively. Taking the more conservative 670/850 nm chromophore concentrations, however, still showed total hemoglobin and ctO_2Hb were approximately 15 and 20% lower ($p < 0.05$) in 3xTg mice, respectively, compared to controls indicating significantly diminished baseline vascular perfusion in the 3xTg mice. This confirms a previous study showing reduced vascular volume in 3xTg mice compared to age-matched controls,[5] as evidenced by radioactive inulin perfusion.

Dynamic Hyperoxia Challenge

To visualize the brain reactivity to hyperoxia, continuous measurements of chromophores and scattering parameters were plotted in a time series as the inhaled gas mixture was changed from 21% O_2 to 100% O_2 (Fig. 4). In this single challenge, a rise in ctO_2Hb and O_2 saturation and a dip in ctHHb were seen. Neurovascular reactivity to hyperoxia challenge was measured from the magnitude differences between baseline

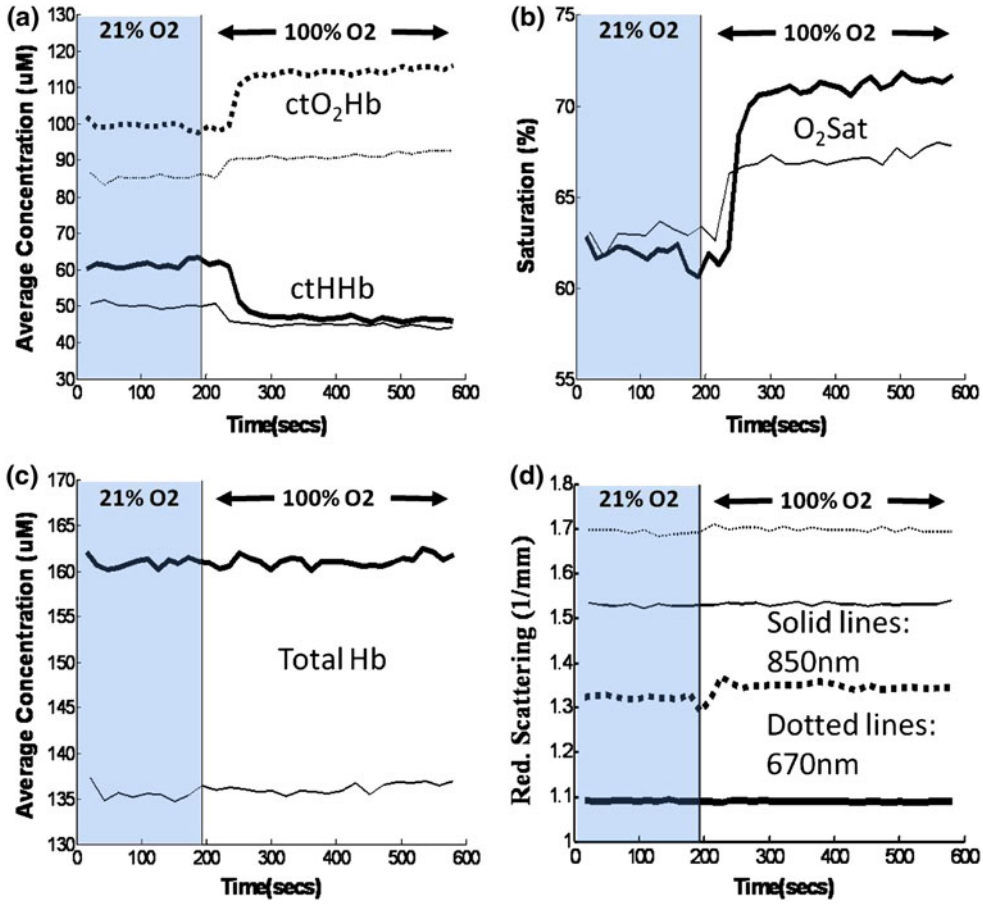

FIGURE 4. Representative dynamic time courses in Alzheimer's (thin lines) and control mice (thick lines) of (a) oxy-hemoglobin (ctO_2Hb, dotted lines) and deoxy-hemoglobin (ctHHb, continuous lines), (b) oxygen saturation (O_2 sat), (c) total hemoglobin (Total Hb), and (d) reduced scattering coefficient at 670 nm (dotted lines) and 850 nm (continuous lines).

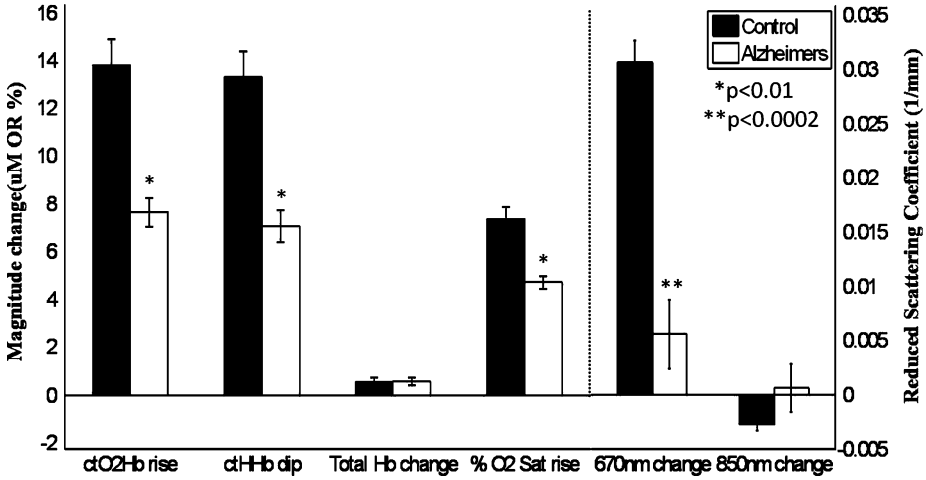

FIGURE 5. Hemoglobin and scattering at 670/850 nm magnitude changes between three min baselines during 21% O_2 and 100% O_2 were reduced in 3xTg mice compared to controls (group average ± group SE).

TABLE 2. Rates of chromophore change, expressed as (mean ± SE) in control (n = 6) and 3xTg (n = 4), measured during hyperoxic challenge.

Subject	ctO_2Hb (μM/s)	ctHHb (μM/s)	Total Hb (μM/s)	O_2 sat (%/s)
Control	0.74 ± 0.05	0.74 ± 0.06	0.04 ± 0.01	0.4 ± 0.02
3xTg	0.32 ± 0.03**	0.24 ± 0.06**	0.02 ± 0.01	0.2 ± 0.02**

**$p < 0.001$.

values and changes in ctO_2Hb, ctHHb, % O_2 saturation, and scattering at 670 nm were significantly attenuated in 3xTg mice (Fig. 5). Furthermore, chromophore dynamics were calculated as the slope at the T_{50}, or halfway point between the two baselines, and found to be twofold to threefold slower in the 3xTg mice (Table 2). In magnitude change and dynamics, the total hemoglobin content in both 3xTg and control mice stayed constant with hyperoxia challenge.

DISCUSSION

This pilot study is the first to concurrently image tissue hemoglobin content and scattering *in vivo* in an AD model. Our results show significantly impaired vascular perfusion in the 3xTg's which corroborates previous 3xTg vascular volume results.[5] At 21% O_2, total Hb and ctO_2Hb levels are about 27 and 39% lower than control, respectively, potentially from Aβ-induced vasoconstriction[19] or impaired angiogenesis and decreased vessel density. The anesthesia agent, isoflurane, is a potent vasodilator[12] and baseline differences in absorption and scattering could also be explained by an attenuated vasodilation response in the 3xTg mice compared to controls. In addition, a 20% differential increase in brain water content in 3xTg mice over controls was observed, potentially indicating edema and decreased cellularity (a significant source of water signals) associated with AD. Our observations of elevated water and reduced hemoglobin content are generally consistent with AD progression which produces neural cell atrophy and concomitant reduction in vascular supply.[31] Histologic vascular formation analyses and tissue biochemical assays, as well as hypercapnia-induced vasodilation studies, are planned for future experiments to further characterize the 3xTg AD mouse model.

The *in vivo* findings of increased NIR scattering in 3xTg mice compared to controls strengthens a previous *ex vivo* human study that showed increased NIR reduced scattering coefficients in post-mortem flash-frozen AD brain samples.[17] The wavelength-dependent scattering spectra revealed a twofold decrease in the scatter pre-factor (A) value and slight (~11%) decrease in scatter power (b) value. The scatter pre-factor is positively correlated with scatterer density and the scatter power is negatively correlated with scatterer size,[35] indicating 3xTg mice on average may have decreased scatterer density and increased scatterer size compared to controls. Overall, elevated scattering values are suggestive of AD neural tissue with higher refractive index particles/discontinuities compared to controls. Although the precise structural origin of the scattering signal is not known, it could be a result of contributions from cellular dystrophies, microgliosis, demyelination, and/or Aβ-induced vasoconstriction and fibrosis found in the 3xTg mice previously.[10,19,24,29] These observations are generally consistent with the absorption-spectra impressions of diminished vascular content, cellular atrophy, and edema.

The absolute scattering measurement accuracy is affected by contributions from the mineral oil and skull, and the imprecision of the light transport model. We used a homogeneous Monte Carlo model because our preliminary experiments on test animals indicated that mineral oil (vs. dry skull) and mineral oil skull (vs. no skull) account for relatively small reductions in scattering (~7 and ~10%, respectively, data not shown), while the physiological benefit of maintaining intact skull in terms of reducing trauma, swelling, and motion artifact is well-established. In addition, the thinness of the mouse's skull (~500 μm) and the small size of the brain (<1 cm) preclude us from rigorously applying a two-layer SFDI analysis as we previously performed in tissue phantom systems, where the upper layer thickness significantly exceeded the transport scattering length.[42] Thus, while relative comparisons between AD and control mice are valid for a given anesthesia agent/dose, characterization of absolute values requires further technology and animal model development.

Supplementing the observed static absorption and scattering contrast our results show for the first time that a hyperoxia challenge can be used to reveal dynamic contrast in AD mice. Hyperoxia is known to induce microvascular vasoconstriction, possibly through prostaglandin synthesis inhibition or reactive oxygen species formation.[32] However, SFDI was not sensitive to these microvascular changes as seen by lack of total hemoglobin changes. Both AD and control mice showed an expected increase in ctO_2Hb and symmetric drop in ctHHb due to enhanced delivery of HbO_2. However, the same challenge produced twofold less increase in ctO_2Hb in 3xTg mice. This offers an additional sensitive metric in which a lower vascular volume would limit increase in blood oxygenation, and it confirms the baseline results that vascular perfusion is impaired in the AD mice.

Surprisingly, a small increase in 670 nm scattering was observed in controls vs. 3xTg mice in response to the hyperoxia challenge, while 850 nm scattering changed little. While tissue scattering could change in response to alterations in intra- vs. extracellular water content,[15] and this balance may be perturbed by gas inhalation challenges, the small changes in scattering values may also be an artifact of absorption crosstalk since incomplete separation of μ_a from μ_s' is particularly problematic under conditions of high absorption (i.e., 670 nm).[8]

In summary, 3xTg baseline ctO_2Hb and total Hb were 61 and 73% of normal, respectively, and we show averages of 13–26% higher scattering contrast values (650–970 nm) in resting AD brains *in vivo* for the first time. Both the magnitude and rate of change of chromophore signals to hyperoxia challenge are substantially reduced in 20-month-old 3xTg subjects compared to age-matched controls, suggesting neurovascular reactivity impairment in AD mice. These preliminary results are limited because of the small sample size and the need to include additional age groups to definitively characterize the effects of normal aging. Nevertheless, we have demonstrated that SFDI is sensitive to intrinsic tissue optical properties that can be obtained *in vivo* to distinguish AD-induced brain pathology from age-matched controls. The structural and functional origin-of-contrast is consistent with previously reported studies, and SFDI may be useful in quantifying spatial and temporal features of AD appearance, progression, and response to therapy. In addition, because optical contrast obtained from SFDI in animal models can be correlated to diffuse optical tomography (DOT) and f-MRI brain imaging studies in humans, this approach provides a platform to inform further clinical translational studies in humans.

ACKNOWLEDGMENTS

This work was supported by the NIH Laser and Microbeam Medical Program (LAMMP P41-RR01192) the Beckman Foundation, and NIH National Institute of Aging (R01 A6-21982). We would like to thank Mr. Bruce Yang, M.S., for machining the mouse ear bars, and A.J. Lin is grateful for the support of the NIH-funded UC Irvine Medical Scientist Training Program (MSTP).

CONFLICT OF INTEREST

The authors (B.J.T., F.M.L., K.N.G.) have received or will receive benefits for personal or professional use from commercial parties related directly or indirectly to the subject of this manuscript.

OPEN ACCESS

REFERENCES

[1]Abookasis, D., C. C. Lay, M. S. Mathews, M. E. Linskey, R. D. Frostig, and B. J. Tromberg. Imaging cortical absorption, scattering, and hemodynamic response during ischemic stroke using spatially modulated near-infrared illumination. *J. Biomed. Opt.* 14(2):024033, 2009.

[2]Ayata, C., A. K. Dunn, O. Y. Gursoy, Z. Huang, D. A. Boas, and M. A. Moskowitz. Laser speckle flowmetry for

the study of cerebrovascular physiology in normal and ischemic mouse cortex. *J. Cereb. Blood Flow Metab.* 24(7):744–755, 2004.

[3]Ayers, F. R., D. J. Cuccia, K. M. Kelly, and A. J. Durkin. Wide-field spatial mapping of in vivo tattoo skin optical properties using modulated imaging. *Lasers Surg. Med.* 41(6):442–453, 2009.

[4]Boas, D. A., and A. K. Dunn. Laser speckle contrast imaging in biomedical optics. *J. Biomed. Opt.* 15(1):011109, 2010.

[5]Bourasset, F., O. Melissa, C. Tremblay, C. Julien, T. M. Do, S. Oddo, F. LaFerla, and F. Calon. Reduction of the cerebrovascular volume in a transgenic mouse model of Alzheimer's disease. *Neuropharmacology* 56(4):808–813, 2009.

[6]Cerussi, A. E., D. Jakubowski, N. Shah, F. Bevilacqua, R. Lanning, A. J. Berger, D. Hsiang, J. Butler, R. F. Holcombe, and B. J. Tromberg. Spectroscopy enhances the information content of optical mammography. *J. Biomed. Opt.* 7(1):60–71, 2002.

[7]Chen-Bee, C. H., D. B. Polley, B. Brett-Green, N. Prakash, M. C. Kwon, and R. D. Frostig. Visualizing and quantifying evoked cortical activity assessed with intrinsic signal imaging. *J. Neurosci. Methods* 97(2):157–173, 2000.

[8]Cuccia, D. J., F. Bevilacqua, A. J. Durkin, F. R. Ayers, and B. J. Tromberg. Quantitation and mapping of tissue optical properties using modulated imaging. *J. Biomed. Opt.* 14(2):024012, 2009.

[9]Cuccia, D. J., F. Bevilacqua, A. J. Durkin, and B. J. Tromberg. Modulated imaging: quantitative analysis and tomography of turbid media in the spatial-frequency domain. *Opt. Lett.* 30(11):1354–1356, 2005.

[10]Desai, M. K., K. L. Sudol, M. C. Janelsins, M. A. Mastrangelo, M. E. Frazer, and W. J. Bowers. Triple-transgenic Alzheimer's disease mice exhibit region-specific abnormalities in brain myelination patterns prior to appearance of amyloid and tau pathology. *Glia* 57(1):54–65, 2009.

[11]Dickstein, D. L., K. E. Biron, M. Ujiie, C. G. Pfeifer, A. R. Jeffries, and W. A. Jefferies. Abeta peptide immunization restores blood-brain barrier integrity in Alzheimer disease. *FASEB J.* 20(3):426–433, 2006.

[12]Franceschini, M. A., H. Radhakrishnan, K. Thakur, W. Wu, S. Ruvinskaya, S. Carp, and D. A. Boas. The effect of different anesthetics on neurovascular coupling. *Neuroimage* 51(4):1367–1377, 2010.

[13]Frostig, R. D. In vivo Optical Imaging of Brain Function (2nd ed.). Boca Raton: CRC Press, 2009.

[14]Garcia-Allende, P. B., V. Krishnaswamy, P. J. Hoopes, K. S. Samkoe, O. M. Conde, and B. W. Pogue. Automated identification of tumor microscopic morphology based on macroscopically measured scatter signatures. *J. Biomed. Opt.* 14(3):034034, 2009.

[15]Gill, A. S., K. F. Rajneesh, C. M. Owen, J. Yeh, M. Hsu, and D. K. Binder. Early optical detection of cerebral edema in vivo. *J. Neurosurg.* 114(2):470–477, 2011.

[16]Gonzalez-Velasquez, F. J., J. A. Kotarek, and M. A. Moss. Soluble aggregates of the amyloid-beta protein selectively stimulate permeability in human brain microvascular endothelial monolayers. *J. Neurochem.* 107(2):466–477, 2008.

[17]Hanlon, E. B., L. T. Perelman, E. I. Vitkin, F. A. Greco, A. C. McKee, and N. W. Kowall. Scattering differentiates Alzheimer disease in vitro. *Opt. Lett.* 33(6):624–626, 2008.

[18]Kassner, A., J. D. Winter, J. Poublanc, D. J. Mikulis, and A. P. Crawley. Blood-oxygen level dependent MRI measures of cerebrovascular reactivity using a controlled respiratory challenge: reproducibility and gender differences. *J. Magn. Reson. Imaging* 31(2):298–304, 2010.

[19]Khalil, Z., H. Poliviou, C. J. Maynard, K. Beyreuther, C. L. Masters, and Q. X. Li. Mechanisms of peripheral microvascular dysfunction in transgenic mice overexpressing the Alzheimer's disease amyloid Abeta protein. *J. Alzheimers Dis.* 4(6):467–478, 2002.

[20]Konecky, S. D., A. Mazhar, D. Cuccia, A. J. Durkin, J. C. Schotland, and B. J. Tromberg. Quantitative optical tomography of sub-surface heterogeneities using spatially modulated structured light. *Opt. Express* 17(17):14780–14790, 2009.

[21]Lajtha, A., G. E. Gibson, and G. A. Dienel. Handbook of Neurochemistry and Molecular Neurobiology. Brain Energetics, Integration of Molecular and Cellular Processes (3rd ed.). New York: Springer, 2007.

[22]Lay, C. C., M. F. Davis, C. H. Chen-Bee, and R. D. Frostig. Mild sensory stimulation completely protects the adult rodent cortex from ischemic stroke. *PLoS One* 5(6):e11270, 2010.

[23]Marshall, S. A., P. Nyquist, and W. C. Ziai. The role of transcranial Doppler ultrasonography in the diagnosis and management of vasospasm after aneurysmal subarachnoid hemorrhage. *Neurosurg. Clin. N. Am.* 21(2):291–303, 2010.

[24]Mastrangelo, M. A., and W. J. Bowers. Detailed immunohistochemical characterization of temporal and spatial progression of Alzheimer's disease-related pathologies in male triple-transgenic mice. *BMC Neurosci.* 9:81, 2008.

[25]Mazhar, A., D. J. Cuccia, S. Gioux, A. J. Durkin, J. V. Frangioni, and B. J. Tromberg. Structured illumination enhances resolution and contrast in thick tissue fluorescence imaging. *J. Biomed. Opt.* 15(1):010506, 2010.

[26]McDonald, R. J., L. A. Craig, and N. S. Hong. The etiology of age-related dementia is more complicated than we think. *Behav. Brain Res.* 214:3–11, 2010.

[27]Meyer, E. P., A. Ulmann-Schuler, M. Staufenbiel, and T. Krucker. Altered morphology and 3D architecture of brain vasculature in a mouse model for Alzheimer's disease. *Proc. Natl. Acad. Sci. USA* 105(9):3587–3592, 2008.

[28]Mulvey, C. S., C. A. Sherwood, and I. J. Bigio. Wavelength-dependent backscattering measurements for quantitative real-time monitoring of apoptosis in living cells. *J. Biomed. Opt.* 14(6):064013, 2009.

[29]Olabarria, M., H. N. Noristani, A. Verkhratsky, and J. J. Rodriguez. Concomitant astroglial atrophy and astrogliosis in a triple transgenic animal model of Alzheimer's disease. *Glia* 58(7):831–838, 2010.

[30]Pavics, L., F. Grunwald, K. Reichmann, T. Sera, E. Ambrus, R. Horn, A. Hartmann, C. Menzel, L. Csernay, and H. J. Biersack. rCBF SPECT and the acetazolamide test in the evaluation of dementia. *Nucl. Med. Rev. Cent. East Eur.* 1(1):13–19, 1998.

[31]Querfurth, H. W., and F. M. LaFerla. Alzheimer's disease. *N. Engl. J. Med.* 362(4):329–344, 2010.

[32]Rousseau, A., E. Tesselaar, J. Henricson, and F. Sjoberg. Prostaglandins and radical oxygen species are involved in microvascular effects of hyperoxia. *J. Vasc. Res.* 47(5):441–450, 2010.

[33]Shin, H. K., P. B. Jones, M. Garcia-Alloza, L. Borrelli, S. M. Greenberg, B. J. Bacskai, M. P. Frosch, B. T. Hyman, M. A. Moskowitz, and C. Ayata. Age-dependent cerebrovascular dysfunction in a transgenic mouse model of cerebral amyloid angiopathy. *Brain* 130(Pt 9):2310–2319, 2007.

[34]Silvestrini, M., P. Pasqualetti, R. Baruffaldi, M. Bartolini, Y. Handouk, M. Matteis, F. Moffa, L. Provinciali, and

F. Vernieri. Cerebrovascular reactivity and cognitive decline in patients with Alzheimer disease. *Stroke* 37(4): 1010–1015, 2006.

[35]Srinivasan, S., B. W. Pogue, S. Jiang, H. Dehghani, C. Kogel, S. Soho, J. J. Gibson, T. D. Tosteson, S. P. Poplack, and K. D. Paulsen. Interpreting hemoglobin and water concentration, oxygen saturation, and scattering measured in vivo by near-infrared breast tomography. *Proc. Natl. Acad. Sci. USA* 100(21):12349–12354, 2003.

[36]Stefani, A., G. Sancesario, M. Pierantozzi, G. Leone, S. Galati, A. H. Hainsworth, and M. Diomedi. CSF biomarkers, impairment of cerebral hemodynamics and degree of cognitive decline in Alzheimer's and mixed dementia. *J. Neurol. Sci.* 283(1–2):109–115, 2009.

[37]Stoppe, G., R. Schutze, A. Kogler, J. Staedt, D. L. Munz, D. Emrich, and E. Ruther. Cerebrovascular reactivity to acetazolamide in (senile) dementia of Alzheimer's type: relationship to disease severity. *Dementia* 6(2):73–82, 1995.

[38]Tanner, K., E. D'Amico, A. Kaczmarowski, S. Kukreti, J. Malpeli, W. W. Mantulin, and E. Gratton. Spectrally resolved neurophotonics: a case report of hemodynamics and vascular components in the mammalian brain. *J. Biomed. Opt.* 10(6):064009, 2005.

[39]Tromberg, B. J., B. W. Pogue, K. D. Paulsen, A. G. Yodh, D. A. Boas, and A. E. Cerussi. Assessing the future of diffuse optical imaging technologies for breast cancer management. *Med. Phys.* 35(6):2443–2451, 2008.

[40]Vicenzini, E., M. C. Ricciardi, M. Altieri, F. Puccinelli, N. Bonaffini, V. Di Piero, and G. L. Lenzi. Cerebrovascular reactivity in degenerative and vascular dementia: a transcranial Doppler study. *Eur. Neurol.* 58(2):84–89, 2007.

[41]Wang, X., B. W. Pogue, S. Jiang, X. Song, K. D. Paulsen, C. Kogel, S. P. Poplack, and W. A. Wells. Approximation of Mie scattering parameters in near-infrared tomography of normal breast tissue in vivo. *J. Biomed. Opt.* 10(5): 051704, 2005.

[42]Weber, J. R., D. J. Cuccia, and B. J. Tromberg. Modulated imaging in layered media. *Conf. Proc. IEEE Eng. Med. Biol. Soc.* Suppl:6674–6676, 2006.

[43]Yezhuvath, U. S., J. Uh, Y. Cheng, K. Martin-Cook, M. Weiner, R. Diaz-Arrastia, M. van Osch, and H. Lu. Forebrain-dominant deficit in cerebrovascular reactivity in Alzheimer's disease. *Neurobiol. Aging*. doi:10.1016/j.neurobiolaging.2010.02.005.

[44]Zhang, X., and W. Le. Pathological role of hypoxia in Alzheimer's disease. *Exp. Neurol.* 223(2):299–303, 2010.